RESEARCH ARTICLE SUMMARY

IMMUNOMETABOLISM

γδ T cells regulate the intestinal response to nutrient sensing

Zuri A. Sullivan, William Khoury-Hanold, Jaechul Lim, Chris Smillie, Moshe Biton, Bernardo S. Reis, Rachel K. Zwick, Scott D. Pope, Kavita Israni-Winger, Roham Parsa, Naomi H. Philip, Saleh Rashed, Noah Palm, Andrew Wang, Daniel Mucida, Aviv Regev, Ruslan Medzhitov*

INTRODUCTION: The gastrointestinal (GI) tract is a multikingdom cellular ecosystem that facilitates the procurement of nutrients from the environment. In constant contact with the external world, the small intestine is at once a gateway for life-threatening pathogens and toxins and the site of absorption for life-sustaining nutrients. Consequently, this tissue is tasked with the challenge of balancing its primary functions of nutrient uptake and host defense in response to a complex and constantly changing environment.

This challenge is particularly daunting for omnivores, whose diets change on daily, seasonal, and developmental time scales. The diverse diets of such generalists stand in contrast to those of specialists—animals that consume restricted diets—such as carnivores and herbivores. Whereas these specialists have evolved fixed morphologic adaptations in the organization of the GI tract that facilitate efficient nutrient uptake from their restricted diets, generalists must constantly adapt to the shifting availability of food sources of diverse nutrient composition encountered throughout life. These ongoing changes in diet exist alongside encounters with ingested toxins, enteric pathogens, and commensal microbes. Omnivorous lifestyles therefore require that the GI tracts of such animals dynamically adapt to the changes in availability of different nutrients. We examined the molecular and cellular mechanisms that regulate intestinal adaptation to diverse foods.

RATIONALE: We investigated how the enzymes and transporters involved in the digestion and absorption of macronutrients are regulated in response to diet. We designed special animal diets that differed only in the ratio of protein to carbohydrates and evaluated gene expression changes in the GI tract, as well as systemic metabolism, after feeding these diets to mice. Recent discoveries pertaining to intestinal defenses against parasitic and microbial pathogens have demonstrated that interactions between intestinal epithelial cells and lymphocytes—the largest population of lymphocytes in the body—coordinate tissue responses to enteric infection. Guided by these findings, we hypothesized that the regulation of nutrient-handling machinery may involve coordination between tissue-resident lymphocytes and intestinal epithelial cells. Furthermore, recent work investigating mechanisms of host defense in this tissue led us to hypothesize that cellular remodeling of the intestinal epithelium, which occurs in response to certain infections, may also underlie its adaptation to different nutrients.

RESULTS: A carbohydrate transcriptional program comprising enzymes and transporters that mediate the digestion and absorption of carbohydrates was induced on demand in small-intestine epithelial cells in response to carbohydrate availability. The induction of this transcriptional program was specifically due to the availability of carbohydrates and reflected functional changes in nutrient handling at the tissue and systemic levels. Mice fed a high-carbohydrate diet exhibited changes in the frequency of specialized enterocyte subsets. This indicated that functional specialization exists within the enterocyte compartment, which constitutes approximately 80% of the intestinal epithelium. This also suggested that the induction of the carbohydrate transcriptional program involved cellular remodeling of the intestinal epithelium. The induction of this program and corresponding epithelial remodeling occurred rapidly, after only 5 days of high-carbohydrate feeding. Unexpectedly, the on-demand induction of this program required γδ T cells, a population of lymphocytes enriched at barrier surfaces whose biology remains poorly understood. Intestinal γδ T cells were altered by diet, with changes observed in their transcriptome, tissue localization, and behavior. The diet-dependent regulation of this program by γδ T cells involved suppression of a negative regulator, interleukin-22 (IL-22). Thus, we defined an epithelial-lymphocyte circuit that regulates the intestinal response to nutrient sensing and facilitates the adaptation to diverse diets.

CONCLUSION: Our work demonstrates a role for intestinal lymphocytes in regulating the tissue response to dietary nutrients. Together with other studies in the realm of host-pathogen interactions, our results indicate that lymphocyte-epithelial circuits and epithelial remodeling represent general features of how the intestine adapts to environmental change. By linking nutrition and barrier function at both the cellular and molecular levels, these adaptations allow this complex tissue to adjust the balance between nutrient uptake and host defense in response to environmental change. ■

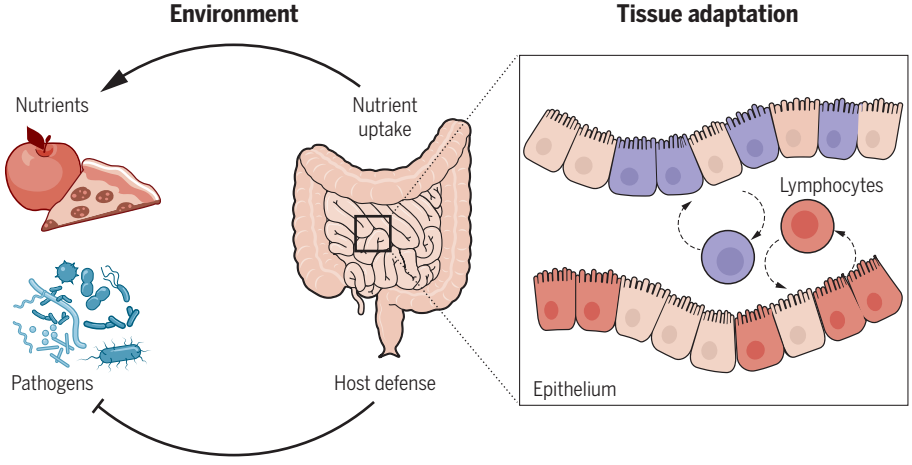

Lymphocyte-epithelial interactions mediate intestinal adaptation to environmental change. The small intestine adjusts the balance between host defense and nutrient uptake in response to environmental signals, including the availability of nutrients and presence of pathogens. The ability of this tissue to adjust the balance between its primary functions in response to environmental cues is mediated through cellular remodeling of the epithelium and lymphocyte-epithelial circuits.

The list of author affiliations is available in the full article online.
*Corresponding author. Email: ruslan.medzhitov@yale.edu
Cite this article as Z. A. Sullivan *et al.*, *Science* **371**, eaba8310 (2021). DOI: 10.1126/science.aba8310

RESEARCH ARTICLE

IMMUNOMETABOLISM

γδ T cells regulate the intestinal response to nutrient sensing

Zuri A. Sullivan[1]*, William Khoury-Hanold[1], Jaechul Lim[1], Chris Smillie[2], Moshe Biton[2]†, Bernardo S. Reis[3], Rachel K. Zwick[4], Scott D. Pope[1,5], Kavita Israni-Winger[1], Roham Parsa[3], Naomi H. Philip[1], Saleh Rashed[1], Noah Palm[1], Andrew Wang[1,6], Daniel Mucida[3], Aviv Regev[2,7,8]‡, Ruslan Medzhitov[1,5]§

The intestine is a site of direct encounter with the external environment and must consequently balance barrier defense with nutrient uptake. To investigate how nutrient uptake is regulated in the small intestine, we tested the effect of diets with different macronutrient compositions on epithelial gene expression. We found that enzymes and transporters required for carbohydrate digestion and absorption were regulated by carbohydrate availability. The "on-demand" induction of this machinery required γδ T cells, which regulated this program through the suppression of interleukin-22 production by type 3 innate lymphoid cells. Nutrient availability altered the tissue localization and transcriptome of γδ T cells. Additionally, transcriptional responses to diet involved cellular remodeling of the epithelial compartment. Thus, this work identifies a role for γδ T cells in nutrient sensing.

Animal diets range in diversity. Specialists rely on a restricted set of food sources, whereas generalists, such as humans and other omnivores, derive nutrition from diverse foods (*1*). For specialists, fixed morphologic adaptations in the organization of the gastrointestinal tract allow for efficient nutrient uptake from restricted food sources (*1*, *2*). By contrast, generalists require dynamic adaptation to the diverse foods that are consumed throughout life. Several features of the small intestine facilitate this flexibility. The mammalian small intestine contains the most lymphocytes of any organ and most neurons outside the brain (*3*, *4*). In addition, the intestinal epithelium turns over every 4 to 5 days and contains various sensory cell types that together make up the gastrointestinal chemosensory system (*5*, *6*). The vast majority of epithelial cells are absorptive enterocytes, which express brush border enzymes and specialized nutrient transporters involved in the uptake of luminal nutrients (*7*, *8*). Equally important in the digestion of dietary nutrients are enzymes secreted from the pancreas into the duodenal lumen. Pancreatic amylases, lipases, and proteases initiate enzymatic digestion of carbohydrates, lipids, and proteins, respectively, after chemical and mechanical digestion in the stomach (*7*, *8*).

The elaborate sensory capacity of the small intestine and rapid turnover of epithelial cells likely confer omnivores with flexibility in the expression of nutrient-handling machinery to maximize digestive efficiency. The loss of lactase expression in adult humans, which gives rise to the phenomenon of lactose intolerance, indicates that this machinery is regulated by substrate availability (*9*). Although individual components of digestive machinery have been demonstrated to be regulated by nutrient availability, whether entire programs can be regulated in this manner and the mechanisms by which these programs are regulated have not been elucidated (*10*–*13*).

Results

Enteric carbohydrate transcriptional program is induced on demand

We tested whether and how nutrient-handling machinery can be dynamically regulated by nutrient availability. Mice were fed isocaloric diets high in either carbohydrates or protein for 5 days, and small-intestine epithelial cells were then analyzed by means of RNA-sequencing (RNA-seq). High-carbohydrate feeding resulted in the up-regulation of the enteric and pancreatic genes involved in the digestion and absorption of dietary carbohydrates (hereafter referred to as "carbohydrate transcriptional program") (Fig. 1, A to C). This program includes pancreatic and brush border enzymes, as well as monosaccharide transporters expressed in absorptive enterocytes (Fig. 1B). Expression of proteases and amino acid transporters was less sensitive to nutrient availability (Fig. 1A), presumably because unlike glucose, which can be generated endogenously through gluconeogenesis and glycogenolysis, essential amino acids can only be obtained from the diet.

We next asked whether the regulation of the carbohydrate transcriptional program was due specifically to the availability of carbohydrates rather than differences in availability of proteins. When mice were fed diets matched for protein that differed in the ratio of fat to carbohydrates, we found increased expression of this program in mice fed a high-carbohydrate diet, independent of protein abundance (Fig. 1D). Animals fed a high-carbohydrate diet and treated with acarbose—an α-glucosidase inhibitor that would limit carbohydrate availability for absorption—showed diminished expression of this program (Fig. 1E). Thus, carbohydrate availability drives the expression of the carbohydrate transcriptional program. The on-demand induction of this program was also preserved in germ-free mice, indicating that it does not require microbial colonization (fig. S1). Last, mice fed a high-carbohydrate diet for 5 days showed more rapid glucose uptake after gavage and increased respiratory quotient compared with mice fed a high-protein diet, indicating that the observed transcriptional changes reflect functional changes in nutrient handling (Fig. 1, F to H).

Two non–mutually exclusive mechanisms could explain the transcriptional changes we observed in response to diet. These changes could arise from direct induction of this transcriptional program in differentiated enterocytes or could involve differentiation of specialized enterocytes that express this program. Although specialized enterocyte subsets have not been previously described, recent reports investigating the intestinal response to infection suggest that epithelial remodeling can underlie transcriptional responses to environmental change in this tissue (*14*–*18*). The induction kinetics of the carbohydrate transcription program were suggestive of epithelial remodeling. In "pulse-chase" experiments, in which mice were fed a high-carbohydrate diet and switched to a high-protein diet for 1 or 5 days, 5-day exposure to the high-protein diet was required for reduction of the carbohydrate transcriptional program (Fig. 2A). Given the 4- to 5-day time scale of small-intestine epithelial turnover, we hypothesized that these kinetics may reflect remodeling of the epithelial compartment in response to nutrient availability. Single-cell RNA-seq (scRNA-seq) of small-intestine epithelial cells from mice that were fed a high-carbohydrate or high-protein diet indicated that a number of epithelial subsets were altered in frequency after 5-day exposure to either of these diets.

[1]Department of Immunobiology, Yale University School of Medicine, New Haven, CT, USA. [2]Klarman Cell Observatory, Broad Institute, Cambridge, MA, USA. [3]Laboratory of Mucosal Immunology, The Rockefeller University, New York, NY, USA. [4]Program in Craniofacial Biology and Department of Orofacial Sciences, University of California, San Francisco, CA, USA. [5]Howard Hughes Medical Institute, New Haven, CT, USA. [6]Division of Rheumatology, Department of Medicine, Yale University School of Medicine, New Haven, CT, USA. [7]The David H. Koch Institute for Integrative Cancer Research at MIT, Department of Biology, Massachusetts Institute of Technology (MIT), Cambridge, MA, USA. [8]Howard Hughes Medical Institute, Cambridge, MA, USA.
*Present address: Department of Molecular and Cellular Biology, Harvard University, Cambridge, MA, USA. †Present address: Department of Biological Regulation, Weizmann Institute of Science, 7610001, Rehovot, Israel. ‡Present Address: Genentech, 1 DNA Way, South San Francisco, CA, USA.
§Corresponding author. Email: ruslan.medzhitov@yale.edu

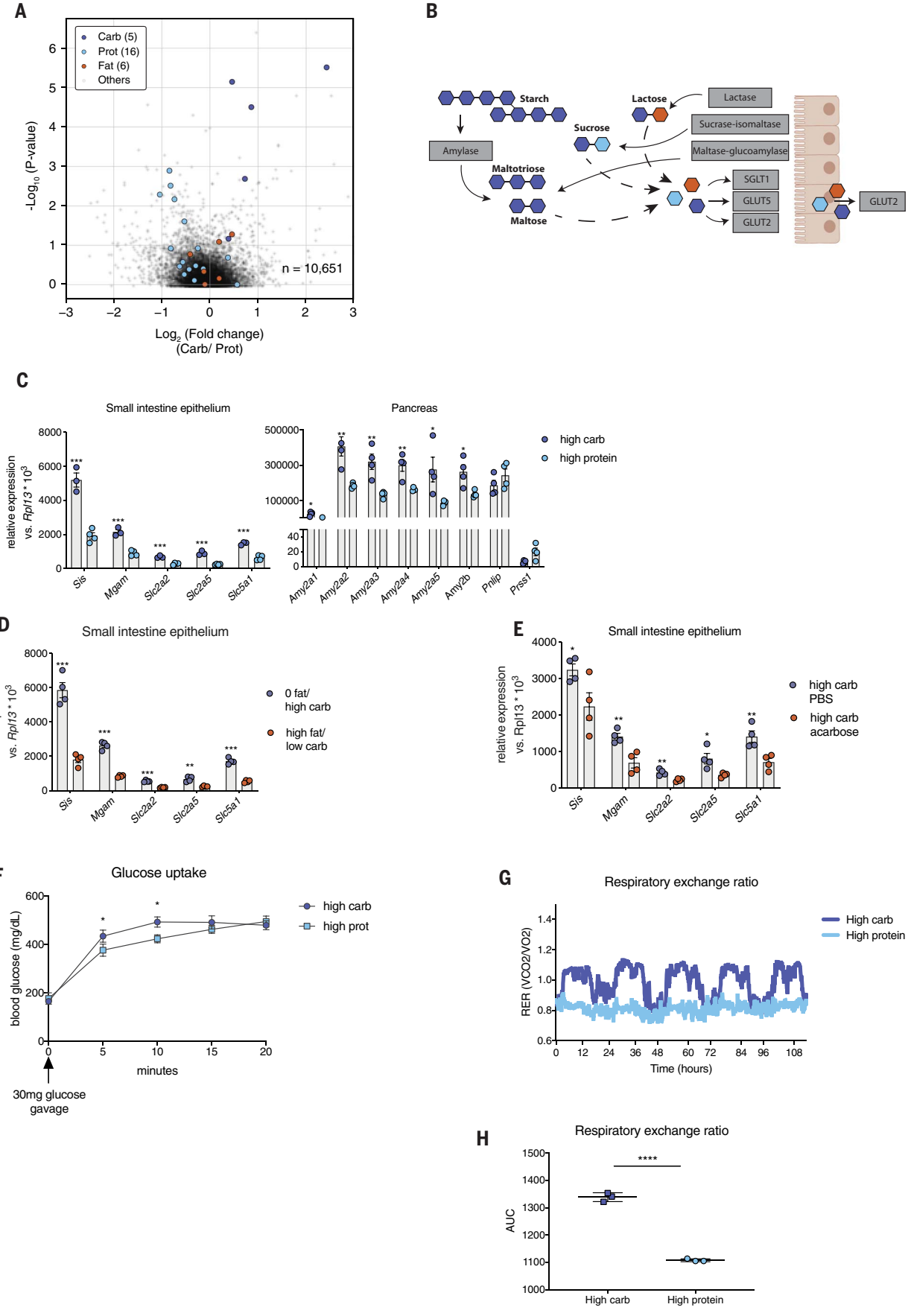

Fig. 1. Carbohydrate availability drives expression of carbohydrate transcriptional program. (**A**) Volcano plot showing differentially regulated genes in small-intestine epithelial cells in response to a high-carbohydrate or high-protein diet. A full list of genes can be found in table S1. Colored circles correspond to transcripts for brush border enzymes and transporters involved in digestion of carbohydrates, protein, or lipids. (**B**) Pancreatic enzymes, brush border enzymes, and monosaccharide transporters involved in digestion and absorption of carbohydrates, encoded by carbohydrate transcriptional program. (**C** to **E**) Quantitative polymerase chain reaction (PCR) analysis of carbohydrate transcriptional program expression in small-intestine epithelium and pancreas of mice fed (C) a high-carbohydrate or high-protein diet, (D) a high-carbohydrate or high-fat diet, or (E) a high-carbohydrate diet and treated with the α-glucosidase inhibitor acarbose. (**F**) Glucose uptake in mice fed a high-carbohydrate or high-protein diet. (**G**) Respiratory exchange ratio and (**H**) corresponding area under the curve in mice fed high-carbohydrate or high-protein diet. n = 3 or 4 mice per group. P values in (A) were calculated by using Sleuth. Data represent mean ± SEM. P values in (B) to (H) were calculated by means of Student's t test. *P < 0.05, **P < 0.01, ***P < 0.001, ****P < 0.0001. Data are representative of at least two independent experiments.

Thus, nutrient availability can likely alter the composition of the small-intestine epithelial compartment (Fig. 2, B to C, and fig. S2). Specifically, a high-carbohydrate diet resulted in a reduction in the frequency of Fabp6$^+$ enterocytes and an increase in the frequency of stem cells (Fig. 2C). Expression of the carbohydrate transcriptional program was enriched in Fabp1$^+$ enterocytes, suggesting that a change in the ratio of Fabp1$^+$ to Fabp6$^+$ enterocytes accounts, at least in part, for the transcriptional changes we observed (Fig. 2D). Enrichment of this program in transit-amplifying cells further suggests that specialized epithelial differentiation underlies its induction. Single-molecule fluorescence in situ hybridization (FISH) experiments revealed intercellular heterogeneity in the expression of the carbohydrate transcriptional program, particularly along the crypt-villus axis (Fig. 2E). One of the components of the carbohydrate transcriptional program, *Slc2a2*, was previously identified as a "landmark" gene for defining spatial heterogeneity in intestinal villi (*19*). This indicated that intercellular heterogeneity in enterocyte nutrient-handling machinery reflects regional patterns in epithelial gene expression along the crypt-villus axis. The phenomenon of small-intestine epithelial remodeling has been observed in the context of other environmental stimuli—specifically bacterial, protozoan, or helminth infection—that promote hyperplasia of secretory epithelial cells involved in host defense (*14*–*18*, *20*). Together with these previous reports, our results suggest that epithelial remodeling may be a general strategy by which the intestine adapts to environmental change.

γδ T cells regulate the carbohydrate transcriptional program

We next investigated whether direct sensing of glucose by epithelial cells was sufficient to drive induction of the carbohydrate transcriptional program. Small-intestine organoids cultured in differing concentrations of glucose did not exhibit robust induction of this program (Fig. 3A). This suggested that direct epithelial sensing was not sufficient to drive activation of this program. TRPM5 (transient receptor potential cation channel subfamily M member 5)–mediated taste receptor signaling and the glucose transporter SGLT1 (sodium/glucose cotransporter 1) were dispensable for induction of this program in vivo (fig. S3). Thus, we considered whether other cell types present in the intestine might contribute to its activation.

The mouse small intestine contains the greatest number of lymphocytes of any tissue, and several recent studies have demonstrated that resident lymphocytes can control epithelial cell fate in response to sensing of enteric infection (*4*, *14*, *16*, *17*). We hypothesized that epithelial-lymphocyte circuitry may also control enteric adaptation to diet. Animals treated with an antibody to Thy1 to deplete T cells and innate lymphoid cells (ILCs) exhibited an impaired induction of the carbohydrate transcriptional program, suggesting the involvement of T cells or ILCs (fig. S4A). The induction of a carbohydrate transcriptional program was also deficient in *Rag2*$^{-/-}$ mice that were fed a high-carbohydrate diet (Fig. 3B). Together, the results in *Rag2*$^{-/-}$ mice (which lack B and T cells), and in mice treated with antibody to Thy1 (which lack ILCs and T cells) indicate the involvement of T cells in regulating the transcriptional response in epithelial cells. Like other barrier tissues, the small intestine contains a large number of both αβ and γδ T cells. Although the role of intestinal αβ T cells in antimicrobial and allergic defense is well established, whether they or γδ T cells play a role in the response to nutrient sensing is unexplored. When we depleted αβ T cells using an antibody to T cell receptor β (TCRβ) or *Tcrb*$^{-/-}$ mice, we found that αβ T cells were dispensable for the induction of this program (Fig. 3C and fig. S4B). By contrast, mice treated with an antibody to TCRγδ or that were genetically deficient in γδ T cells exhibited defective induction of the carbohydrate transcriptional program, with a more robust dependency in antibody-treated animals, presumably owing to developmental compensation in constitutive knockout mice (Fig. 3, D to E). Thus, γδ T cells are required for the induction of nutrient-handling machinery in response to a high-carbohydrate diet.

Intestinal γδ T cells are present in two anatomically and developmentally distinct tissue compartments: the intraepithelial lymphocyte (IEL) and lamina propria (LP) lymphocyte fractions (*21*). IELs are highly abundant and dynamic and interact intimately with epithelial cells (*4*, *20*). By contrast, LP γδ T cells represent a minor fraction of the CD45$^+$ cells in this compartment. Given their proximity to epithelial cells, we hypothesized that IEL γδ T cells would be most responsive to diet. However, when we quantified with microscopy and flow cytometry the number of IELs versus LPLs, we found that LP, not IEL, γδ T cells increased in frequency and number during high-protein feeding (Fig. 3, H and I, and fig. S5). To further investigate the effect of diet on IEL versus LP γδ T cells, we performed intravital imaging studies in *Tcrd*–green fluorescent protein (GFP) mice. LP γδ T cell numbers increased in mice fed a high-protein diet (Fig. 3, H and I, and fig. S5), and IEL γδ T cells exhibited more rapid movement in mice fed a high-carbohydrate diet, suggesting that both γδ T cell compartments are affected by nutrient availability (movie S1). Last, we investigated whether diet might alter the proximity of γδ T cells to the intestinal crypt. We hypothesized that during a high-carbohydrate diet, γδ T cells interact with intestinal epithelial progenitors near the crypt base to drive the transcriptional responses and epithelial remodeling that we observed. Using three-dimensional (3D) tissue imaging, we quantified the relative abundance of γδ T cells along the crypt-villus axis and found an increased frequency of γδ T cells localized close to the crypt base in animals fed a high-carbohydrate diet (fig. S6). Thus, γδ T cells may influence the transcriptome and/or differentiation program of intestinal epithelial cells by interacting with epithelial progenitors in the crypt base.

We then performed RNA-seq on αβ and γδ T cells isolated from intraepithelial and LP compartments. Unlike αβ T cells, γδ T cells from both compartments exhibited significant transcriptional responses to nutrient sensing (Fig. 3, F and G). In particular, the LP γδ T cell compartment showed the greatest number of differentially expressed genes in response to a high-carbohydrate versus high-protein diet (Fig. 3G and tables S3 and S4). Thus, this compartment may be the most sensitive to changes in nutrient availability.

Last, to determine whether intra- or inter-compartmental heterogeneity may play a role in the transcriptional changes that we observed, we performed single-cell RNA-seq on sorted IEL and LP γδ T cells (fig. S7). We identified four transcriptionally distinct clusters of small-intestine

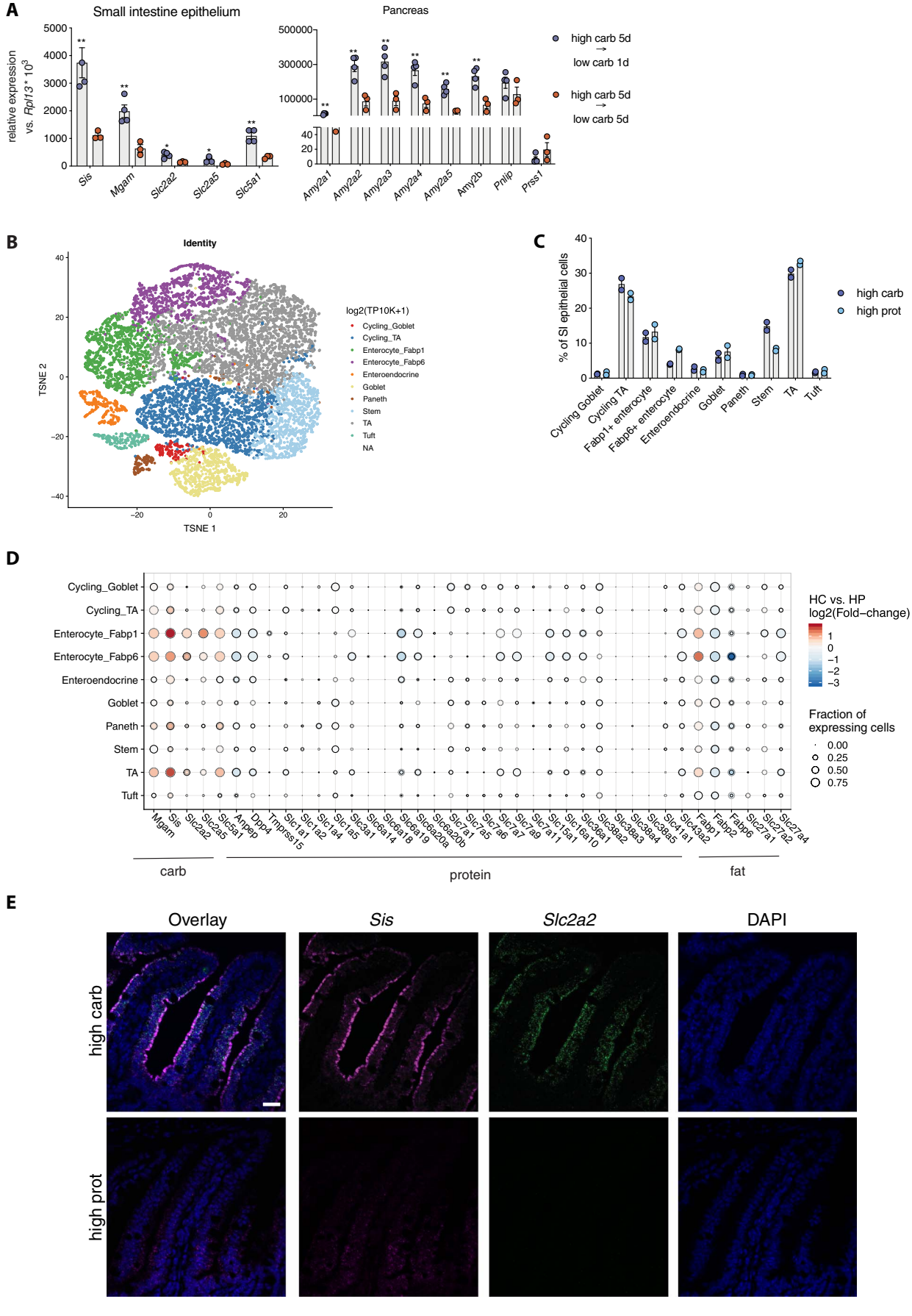

Fig. 2. Diet alters composition of epithelial compartment. (**A**) Expression of carbohydrate transcriptional program in small-intestine epithelium and pancreas in mice fed a high-carbohydrate diet for 5 days and subsequently switched to a high-protein diet for 1 or 5 days. (**B**) *t*-Distributed stochastic neighbor embedding (*t*-SNE) plots of major epithelial cell subsets with 10,000 cells displayed. (**C**) Frequency of epithelial cell subsets in (B) during high-carbohydrate or high-protein diets. (**D**) Differential expression of nutrient-handling machinery for carbohydrates, protein, and fat. A full list of genes can be found in table S2. (**E**) Single-molecule FISH imaging of indicated carbohydrate program transcripts in jejunum isolated from mice fed high-carbohydrate or high-protein diet for 5 days. Scale bar, 100 μm. *P* values in (A) were calculated by using Student's *t* test. Data represent mean ± SEM. $*P < 0.05$, $**P < 0.01$. Data in (A) are representative of at least two independent experiments with $n = 3$ or 4 mice per group. Data in (B) to (D) are from a single experiment, with four mice per group pooled into two samples.

γδ T cells, reflecting intraepithelial and LP compartments (fig. S7A). Although we did not see differences in clustering in response to diet, we observed that one of the clusters we identified was enriched for genes found to be differentially regulated by diet in our bulk-sequencing dataset. Thus, this cluster may be more sensitive to nutrient availability than other enteric γδ T cells (fig. S7, B and C).

We then asked what upstream mediators may signal to γδ T cells during a high-carbohydrate diet. Our sequencing data did not reveal any significant changes in cytokine expression in γδ T cells (fig. S8A). However, contact-dependent signals, including components of Notch signaling, were up-regulated in LP γδ T cells during a high-carbohydrate diet (fig. S8C). We found that *Jag2* (jagged canonical notch ligand 2), a Notch ligand, was up-regulated in epithelial cells in response to a high-carbohydrate diet, suggesting that Notch signaling may mediate communication between γδ T cells and epithelial cells in response to nutrient sensing (fig. S8D). This notion was further supported by our imaging studies, which demonstrated that γδ T cells localize to the crypt base, where Notch ligands are more highly expressed (*22*), during high-carbohydrate feeding (fig. S6). To test whether JAG2/Notch signaling is involved in the induction of the carbohydrate transcriptional program, mice were fed a high-carbohydrate diet and treated with a JAG2-blocking antibody or isotype control. Animals treated with antibody to JAG2 showed diminished expression of the carbohydrate transcriptional program as compared with that of isotype control–treated animals. This suggested that the up-regulation of *Jag2* on epithelial cells during a high-carbohydrate diet played a role in the downstream induction of the carbohydrate transcriptional program (fig. S9A). However, treatment with antibody to JAG2 did not influence the frequency or number of γδ T cells in the IEL or LP compartments (fig. S9, B to D), suggesting that Notch signaling may influence γδ T cell function but not survival.

Our sequencing data also revealed that LP γδ T cells up-regulated *IL2Rb*, the co-receptor for interleukin-2 (IL-2) and IL-15, during high-carbohydrate feeding. This raised the possibility that IL-15 may regulate the γδ T cell response to nutrient sensing (fig. S10A). Animals treated with a blocking antibody to IL-15 showed diminished expression of the carbohydrate transcriptional program as compared with that of isotype control–treated animals, suggesting that IL-15 signaling is an important mediator in this circuit (fig. S10B). Epithelial cell IL-15 expression was not induced by a high-carbohydrate diet, and animals treated with antibody to IL-15 showed no difference in the frequency of IEL or LP γδ T cells. Thus, IL-15 appears to be a tonic signal that maintains γδ T cell function, rather than a nutrient-sensitive signal (fig. S10, C and D).

γδ T cells regulate carbohydrate transcriptional program through control of IL-22

Because we did not find any differentially expressed cytokines in γδ T cells in response to diet, we assessed whether cytokines might be differentially expressed in other cell types. We found that IL-22—a cytokine known to play important roles in regulating metabolism and small-intestine epithelial cell proliferation (*23*–*26*)—was up-regulated in response to a high-protein diet. IL-22 expression was further increased in mice lacking γδ T cells (Fig. 4A). IL-22 was also up-regulated at the protein level. ILC3s, but not T helper 17 (T_H17) cells, showed elevated IL-22 production in response to a high-protein diet and in mice lacking γδ T cells (Fig. 4, B to C, and fig. S11). The increased expression of IL-22 under conditions in which we observed diminished expression of carbohydrate-handling machinery suggested that IL-22 may be a negative regulator of this program. This was confirmed in experiments in which small-intestine organoids were cultured in different concentrations of IL-22. Although small-intestine organoids do not entirely recapitulate the full complement of enterocyte subsets that we observed in vivo, organoids treated with IL-22 showed alterations in the frequency of enterocytes and stem cells similar to the changes we observed in epithelial cells isolated from mice fed different diets (Figs. 2C and 4, D and E). Organoids treated with IL-22 also showed dose-dependent down-regulation of the carbohydrate transcriptional program, confirming that this program is negatively regulated by IL-22 (Fig. 4F). Mice fed a high-protein diet and treated with antibody to IL22 showed expression of the carbohydrate transcriptional program at levels similar to those of mice fed a high-carbohydrate diet (Fig. 4G). Furthermore, treatment with an antibody to TCRγδ was unable to suppress the carbohydrate transcriptional program in *Il22*-deficient animals (Fig. 4H). Thus, γδ T cells regulate the diet-dependent expression of carbohydrate-handling machinery by suppressing expression of IL-22.

Because tuft cells have recently been described to play a critical role in regulating the intestinal response to pathogens, we investigated their role in regulating the intestinal response to nutrient sensing (*14*, *16*, *17*). We found that *Pou2f3*$^{-/-}$ animals, which lack tuft cells, had decreased expression of the carbohydrate transcriptional program, which suggested that tuft cells may be an upstream regulator in this circuit (fig. S12, A and B). IL-25, produced by tuft cells, is known to be a negative regulator of IL-22 expression (*27*). However, we did not see a significant increase in *Il25* expression in intestinal epithelial cells during a high-carbohydrate diet (fig. S12C). We therefore investigated the role of other soluble mediators known to be produced by tuft cells in regulating this circuit. Tuft cells express cyclooxygenase 1 (COX1) and COX2 and are thought to produce prostaglandins (*28*). Because we observed that LP γδ T cells up-regulate prostaglandin receptor during high-carbohydrate feeding (fig. S12D), we treated high-carbohydrate–fed animals with a COX inhibitor, indomethacin. These animals showed marked down-regulation of the carbohydrate transcriptional program (fig. S12E) as well as a trend toward reduced IL-22 (fig. S12F). Thus, tuft cells may be involved in the regulation of the carbohydrate transcriptional program and may control its expression through the production of prostaglandins.

Discussion

Our studies have defined a role for γδ T cells in the regulation of epithelial transcriptional response to diet and showed that diet can alter the frequency of epithelial cell subsets. We found that machinery required for carbohydrate digestion, in both the small intestine and pancreas, can be regulated on demand in response to nutrient availability. IL-22, produced by ILC3s, plays a critical role in the regulation of specialized epithelial cell differentiation and expression of digestive machinery, and γδ T cells can regulate its production. How γδ T cells regulate the production of IL-22 by ILC3s is an important area for future study. A recent study reported that γδ T cell–deficient animals have an increased number of another innate-like lymphocyte, mucosal-associated invariant

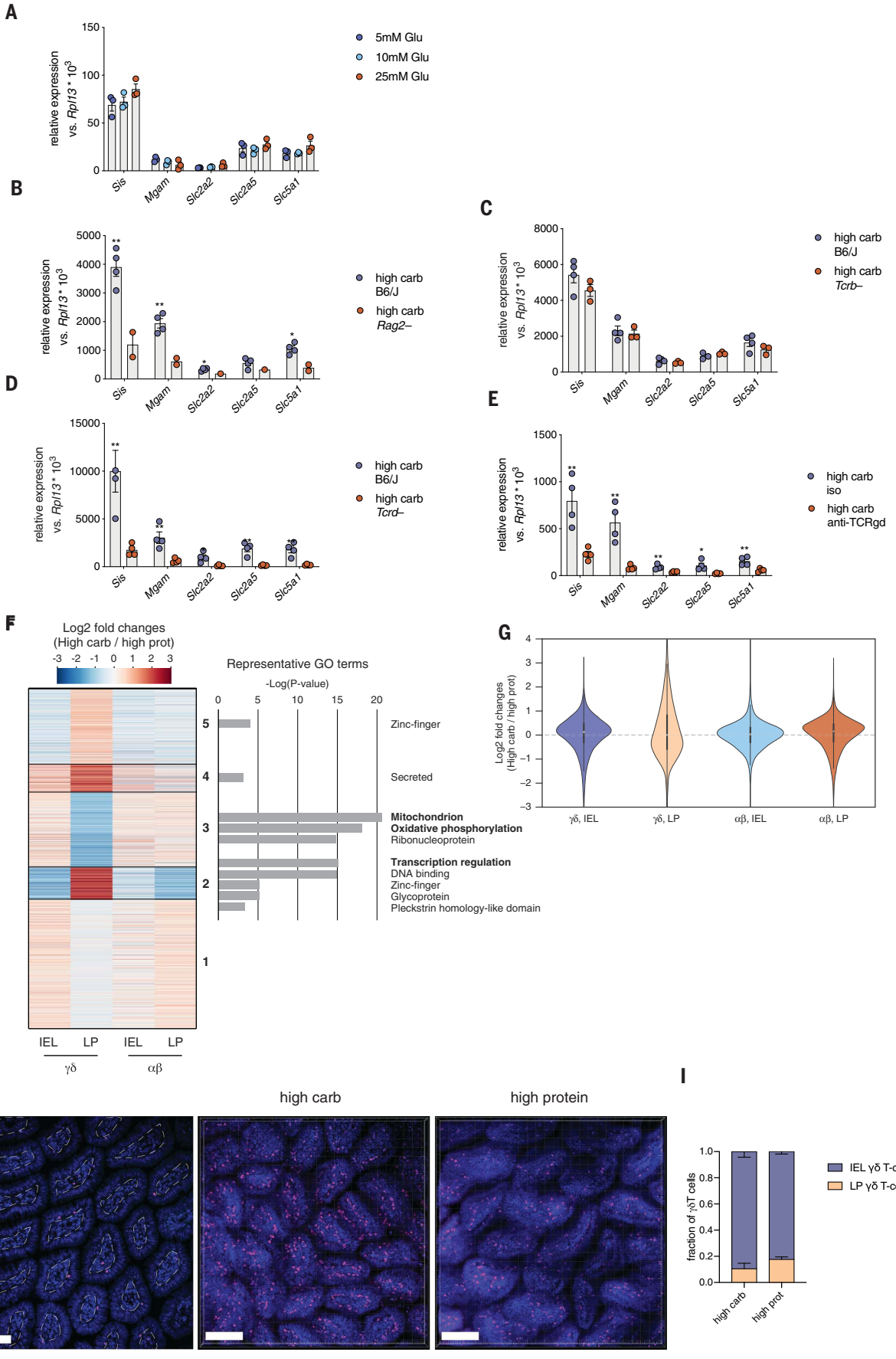

Fig. 3. γδ T cells are required for induction of carbohydrate transcriptional program. (**A**) Expression of the carbohydrate transcriptional program in small-intestine organoids cultured with indicated varying concentrations of glucose. (**B** to **E**) Expression of the carbohydrate transcriptional program in small-intestine epithelial cells from mice fed high-carbohydrate diet under indicated genotypes and treatment conditions. (**F**) Heatmap showing fold changes in transcript levels in LP or IEL γδ or αβ T cells isolated from the small intestine of mice fed a high-carbohydrate or high-protein diet. Genes were grouped by means of *K*-means clustering and functionally analyzed with DAVID (*54*). Full gene lists are available in table S3 (n = 3 or 4 mice per group). (**G**) Transcriptomic reprogramming of γδ T cells in LP. Violin plots show the changes in RNA expression between high-carbohydrate and high-protein diets. The plots were scaled with the same area. The white dot indicates the median. (**H**) Representative images of cleared ileal tissue from *Tcrgd*-GFP mice fed a high-carbohydrate or high-protein diet. Dotted lines indicate the border used to delineate the IEL from LP regions. γδ T cells are pseudocolored red. Scale bar, 100 μm. (**I**) Quantification of LP and IEL γδ T cells from cleared tissue images. n = 3 or 4 mice per group. Data represent mean ± SEM. P values in (A) to (E) were calculated by means of Student's t test. $^*P < 0.05$, $^{**}P < 0.01$. Data are representative of at least two independent experiments, except in (F) and (G), which represent a single sequencing experiment.

T (MAIT) cells, in the small intestine (*29*). This study, as well as our finding that γδ T cells limit intestinal ILC3s, suggest that γδ T cells may restrict other resident innate-like lymphocytes in the intestine. The precise molecular mechanisms that dictate the interrelationships between intestinal innate-like lymphocytes—including MAIT cells, invariant natural killer T cells (iNKT cells), ILCs, and γδ T cells—represent a broad and substantial area for future investigation in mucosal immunity.

This work demonstrates a major role for intestinal γδ T cells outside of antimicrobial defense and adds to emerging evidence of the tissue homeostatic role of γδ T cells (*30*–*33*). Previous studies have pointed to a role for γδ T cells in the pathogenesis of metabolic diseases, indicating that they influence the regulation of blood glucose (*34*–*36*). Our finding provides additional context to these reports, suggesting that γδ T cells may contribute to these pathologies through direct regulation of glucose uptake in the intestine. The relative contributions of antigen recognition by the γδ TCR and recognition of other signals such as butyrophilins to the tissue homeostatic function of γδ T cells is an important area for future study that could be aided by identification of γδ TCR antigens, which have largely remained elusive (*37*–*39*).

Our finding that IL-22 can regulate carbohydrate-handling machinery accords with recent reports of its role in the regulation of lipid uptake machinery in the small intestine (*40*–*42*). Together, these findings may help to link the demonstrated role of IL-22 in organismal metabolism to its function in intestinal epithelial homeostasis and raise the possibility that IL-22 may mediate its effects on metabolism in part through its action on intestinal epithelial cells (*23*–*26*, *40*, *41*). This has large implications for understanding the link between intestinal function and metabolic homeostasis, as well as for current efforts to apply IL-22 as a therapeutic for intestinal injury and metabolic disease. Additionally, IL-22 induction through continuous exposure to enteropathogens may contribute to diseases of nutrient malabsorption, as occurs in environmental enteropathy (*43*).

Together with recent studies of intestinal response to helminth, bacterial, and protozoan infections (*14*–*18*, *20*), our work suggests that epithelial cell–lymphocyte circuits and epithelial remodeling may be general features of adaptability to environmental change in this tissue. Our observation that nutrient uptake can be regulated by lymphocyte control of cytokine production links the regulation of nutrient uptake to the regulation of barrier defense. The finding that shared machinery can regulate both of these crucial functions in the small intestine may help explain how this tissue adjusts the balance between defense and nutrient uptake in the face of constant environmental change. Whether nutrient uptake can be regulated by other intestinal lymphocytes and cytokines in response to different environmental signals is an intriguing question for further investigation.

Materials and methods

Animals

All animal experiments were performed in accordance with institutional regulations after protocol review and approval by Yale University's Institutional Animal Care and Use Committee. The following strains were obtained from Jackson Laboratories: C57BL/6J (stock no. 000664), *Tcrd*$^{-/-}$ (stock no. 002120), *Tcrb*$^{-/-}$ (stock no. 002118), *Il22*$^{-/-}$ (stock no. 027524). *Rag2*$^{-/-}$ mice were provided by D. Schatz (Yale University), *Tcrd*-GFP mice were provided by D. Mucida (Rockefeller University), *Trpm5*$^{-/-}$ mice were provided by W. Garrett (Harvard University), and *Pou2f3*$^{-/-}$ mice were provided by C. Wilen (Yale University). Germ-free C57BL/6 mice were bred and maintained in Class Biologically Clean isolators. Dietary interventions and other experimental procedures were performed in microisolator cages (Isocage P; Techniplast). Females aged 7 to 12 weeks were used for all experiments and were euthanized by cervical dislocation at ZT8.

For antibody treatment experiments, animals were injected intravenously with 500 μg of anti-Thy1 (clone 30H12; BioXCell #BP0066) or anti-keyhole lymphocyanin isotype control (clone LTF-2; BioXCell #BP0090); or 200 μg anti-TCRβ (clone H57-597; BioXCell #BE0102), anti-TCRγδ (clone UC7-1365: BioXCell #BE0070), or Armenian hamster isotype control (BioXCell #BE0091) on days −1, 0, 2, and 4 of each experiment. One hundred micrograms of anti-IL-22 (clone IL22JOP; ThermoFisher #16-7222-82) or Rat IgG2a isotype control (clone eBR2a; ThermoFisher #16-4321-82) was injected intraperitoneally on days 0, 2, and 4 of each experiment.

SGLT1 inhibitor phloridzin (SigmaAldrich) was administered subcutaneously every 12 hours for the duration of each experiment. Animals received 5 mg of phloridzin or vehicle (10% EtOH, 15% DMSO, 75% PBS) per injection. Acarbose (Cayman Chemical Co) was administered by daily gavage for the duration of the experiment. Animals received 25 μg acarbose or PBS per treatment. To quantify glucose uptake, animals were fasted for 4 hours and then administered 30 mg of D-glucose by gavage. Blood glucose was measured every 5 min following injection using a OneTouch handheld glucometer. For metabolic cage experiments, animals were individually housed in Promethion High-Definition Multiplexed Respirometry Cages (Sable Systems International). After 3 days of acclimatization, special diets were introduced, and animals were monitored for VO_2 and VCO_2 for 5 days. Purified, specialized animal diets were purchased from Envigo. Diet ingredients and nutritional information are summarized in table S5. Diets were sterilized by irradiation.

Epithelial cell and lamina propria isolation (for qPCR and flow cytometry)

Single-cell suspensions of small intestine epithelium and lamina propria were prepared as described (*44*). Briefly, the small intestine was isolated and opened longitudinally. Its contents were then rinsed in PBS following removal of Peyer's patches. The tissue was then cut into 2-3-mm segments and incubated in RPMI media (ThermoFisher) containing 5 mM EDTA, 145 μg/ml DTT, and 3% FBS at 37°C with 5% CO_2 for 20 min with agitation. Pieces of intestine were then washed in RPMI containing 2 mM EDTA to separate the epithelial fraction. Epithelial cell RNA was isolated from this fraction. In cases where IELs were stained, the epithelial fraction was subjected to 30% Percoll density gradient by centrifugation (Sigma Aldrich). Lamina propria digestion was performed using 100 μg/ml Liberase (Roche) and 500 μg/ml DNAse (Sigma Aldrich) in RPMI

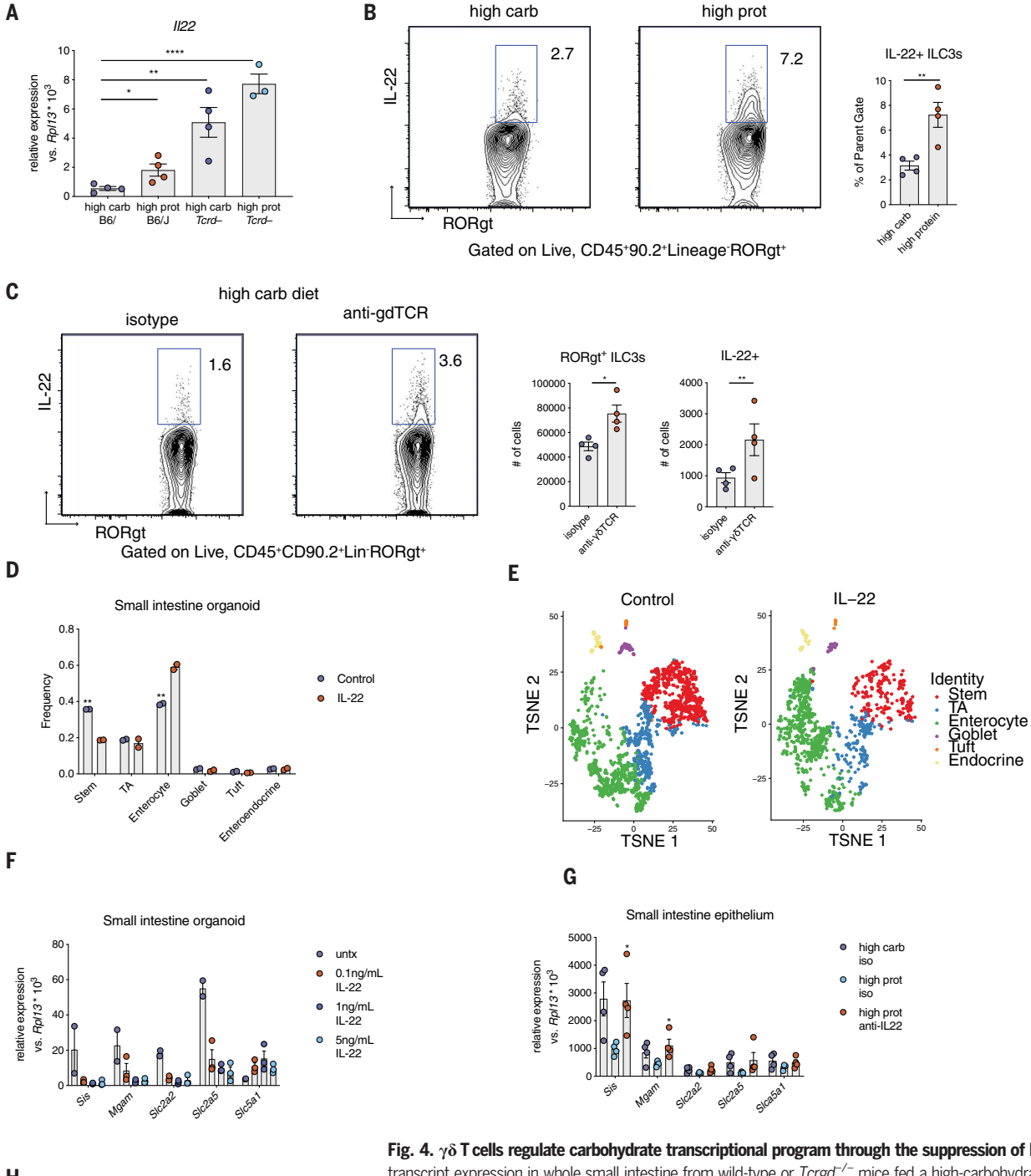

Fig. 4. γδ T cells regulate carbohydrate transcriptional program through the suppression of IL-22. (**A**) *Il22* transcript expression in whole small intestine from wild-type or *Tcrgd*$^{-/-}$ mice fed a high-carbohydrate or high-protein diet. (**B**) Representative intracellular cytokine staining and (right) quantification of IL-22 production in small-intestine ILC3s from mice fed high-carbohydrate or high-protein diets. (**C**) (Left) Representative intracellular cytokine staining and (right) quantification of retinoid-related orphan receptor–γT (RORγT) expression and IL-22 production in small-intestine ILC3s from mice fed a high-carbohydrate diet and treated with antibody to TCRγδ or isotype control. (**D**) Frequency and (**E**) *t*-SNE plots showing epithelial subtypes in small-intestine organoids treated with IL-22 or control media. (**F**) Expression of the carbohydrate transcriptional program in small-intestine organoids treated with indicated concentration of IL-22. (**G**) Expression of the carbohydrate transcriptional program in small-intestine epithelium of mice fed a high-carbohydrate or high-protein diet and treated with antibody to IL22 or isotype control. (**H**) Expression of carbohydrate transcriptional program small-intestine epithelial cells isolated from IL-22–deficient mice fed a high-carbohydrate diet and treated with antibody to TCRγδ or isotype control. n = 3 or 4 mice per group. Data represent mean ± SEM. P values [except in (E)] were calculated by means of Student's t test. P values in (E) were calculated by means of Dirichlet-multinomial regression. *P < 0.05, **P < 0.01, ****P < 0.0001. All data are representative of at least two independent experiments, except (D) and (E), which represent a single sequencing experiment.

for 30 min at 37°C with 5% CO_2. Digested tissue was sequentially strained through 70 μM and 40 μM strainers, washed in RPMI containing 3% FBS, and cells stained for further analysis. Epithelial cells used for scRNAseq were isolated as described (*18*). Small intestines were isolated, opened longitudinally, and rinsed in cold PBS. Two-millimeter tissue fragments were incubated in 20 mM EDTA in PBS for 2-3 hours. The single-cell suspension was then passed through a 40-μm filter and stained for isolation by fluorescence-activated cell sorting (FACS) (Astrios) for droplet-based scRNA-seq (described below).

Flow cytometry

Single-cell suspensions were treated with anti-CD16/32 (Fcblock) (ThermoFisher #14-9161-73) and stained with ZombieYellow Fixable Live/Dead dye (Biolegend #423104) and the following antibodies at a concentration of 1 μg/ml except where otherwise indicated: PE-Cy7-anti-CD326/EpCAM (clone 9C4; Biolegend #118216), BUV395-anti-CD45 (clone 30-F11; BD Biosciences #564279), PE-anti-TCRγδ (clone GL3; ThermoFisher #12-5711-82), APC-anti-TCRβ (clone H57-597; Biolegend #109212), PE-Cy7-anti-TCRβ (clone H57-597; Biolegend #109221), FITC-anti-CD90.2 (clone 30-H12; BD Biosciences 553012) at 2.5 μg/ml, APC-anti-CD90.2 (clone 5302.1; ThermoFisher 17-0902-81), BV605-anti-CD4 (clone RM4-5; Biolegend #100547), 7AAD (ThermoFisher #V35123), anti-PE-anti-CD31 (clone 390; ThermoFisher #12-0311-82), AlexaFluor 647-anti-IL-22 at 2 μg/ml (clone IL22JOP; ThermoFisher #17-7222-80), PE-anti-RORgt at 2 μg/ml (clone B2D; ThermoFisher #E14326-107). "Lineage" staining was performed using PE-Cy7-Streptavidin at 0.5 μg/ml (ThermoFisher #25-4317-82) or BV421-Streptavidin at 0.33 μg/ml (BD Biosciences #563259) and the following biotinylated antibodies at 1.67 μg/ml: anti-CD3 (clone 145-2C11; ThermoFisher #13-0031-85), anti-CD5 (clone 53-7.3; BD Biosciences #553018), anti-CD8a (clone 53-6.7; ThermoFisher #13-0081-82), anti-CD19 (clone 1D3; BD Biosciences #553784), anti-CD11b (clone M1/70; ThermoFisher #13-0112-85), anti-CD11c (clone N418; ThermoFisher #13-0114-82), anti-CD45R (clone RA3-6B; Biolegend #103204), anti-CD49b (clone DX5; BD Biosciences #553856), anti-F4/80 (clone BM8; ThermoFisher #13-4801-85), anti-FcER1 (clone MAR-1; ThermoFisher 13-5898-85), anti-Gr1 (clone RB6-8C5; ThermoFisher #13-5931-85), anti-Nk1.1 (clone PK136; ThermoFisher #13-5941-82), anti-Ter119 (clone TER-119; ThermoFisher #13-5921-81). Stimulation and intracellular cytokine staining were performed as previously described (*44*). Cells were stimulated for 2 hours at 37°C with 50 ng/ml phorbol 12-myristate 13-acetate (Sigma Aldrich) and 3.35 μM ionomycin (Cell Signaling Technologies) in the presence of GolgiPlug (BD Biosciences). Staining for intracellular cytokines and transcription factors was performed using FoxP3/Transcription Factor Staining Buffer Set (ThermoFisher). Flow cytometry was performed using a BD LSRII analyzer equipped with the following lasers: 355 nm (UV), 405 nm (violet), 488 nm (blue), and 633 nm (red). Data were analyzed using FlowJoX (BD Biosciences). Gates were drawn according to fluorescence minus one (FMO) controls.

Cell sorting

For bulk T cell RNA-seq

Stained cells were sorted using a BD FACSAriaII. Cells were gated on live, $CD45^+$, $EpCAM^-$, single-cells, and sorted into $TCR\beta^+TCR\gamma\delta^-$ and $TCR\beta^-TCR\gamma\delta^+$ populations. Cells were collected in RLT lysis buffer (Qiagen) containing 1% beta-mercaptoethanol.

For plate-based scRNA-seq

Cells were sorted using parameters described above. Single γδ T cells were sorted into individual wells of a 96-well plate containing TCL lysis buffer (Qiagen) with 1% β-mercaptoethanol. Immediately after sorting, plates were spun down and frozen at −80°C until library preparation.

For droplet based scRNAseq

FACS (Astrios) was used to sort cells into Eppendorf tubes containing PBS with 0.1% BSA and stored on ice until library preparation. Cells were gated on live, single $CD31^-$ $Ter119^-$ $CD45^-EpCAM^+$ cells.

qPCR analysis

Total RNA was purified from epithelial cells using DiretZol RNA Miniprep Plus Kit (Zymo). Total RNA was purified from organoids using RNEasy Plus Micro Kit (Qiagen). Total RNA was quantified by NanoDrop (ThermoFisher) and added to reverse transcriptase reaction using SMART MMLV Reverse Transcriptase (Takara Bio) according to the manufacturer's instructions. qPCR was performed with PerfeCTa SYBR Green (Quanta Bio) using BioRad CFX96 platform. Expression was calculated relative to *Rpl13a*. A list of primers is provided in table S6.

Intestinal organoid cultures

Crypts were isolated from whole small intestine as follows. The small intestine was extracted and rinsed in cold PBS. The tissue was opened longitudinally and sliced into small fragments roughly 0.2 cm long. The tissue was incubated in 20 mM EDTA-PBS on ice for 90 min, while shaking every 30 min. The tissue was then shaken vigorously and the supernatant was collected as a fraction in a new conical tube. Next, the tissue was incubated in fresh EDTA-PBS and a new fraction was collected every 30 min. Fractions were collected until the supernatant consisted almost entirely of crypts. The final fraction (enriched for crypts) was filtered through a 70-μm filter, washed twice in PBS, centrifuged at 300*g* for 3 min, and dissociated with TrypLE Express (Invitrogen) for 1 min at 37°C. Following crypt isolation from the whole small intestine of both male and female mice, the single-cell suspension was resuspended in Matrigel (BD Bioscience) with 1 μM Jagged-1 peptide (Ana-Spec). Roughly 300 crypts embedded in 25 μl of Matrigel were seeded onto each well of a 24-well plate. Once solidified, the Matrigel was incubated in 600 μl culture medium (Advanced DMEM/F12, Invitrogen) with streptomycin–penicillin and glutamatax and supplemented with EGF (100 ng/ml, Peprotech), R-Spondin-1 (600 ng/ml, R&D), Noggin (100 ng/ml, Prepotech), Y-276432 dihydrochloride monohydrate (10 μM, Tochris), N-acetyl-1-cysteine (1 μM, Sigma-Aldrich), N2 (1X, Life Technologies), B27 (1X, Life Technologies), and Wnt3A (25 ng/ml, R&D Systems). Fresh media was replaced on day 3 and organoids were passaged by dissociation with TrypLE and resuspended in new Matrigel on day 6 with a 1:3 split ratio.

Intravital imaging

The terminal ilea of live *Tcrgd*-GFP mice were imaged as described previously (*20*). Animals were anesthetized using isoflurane before surgery and injected intravenously with Hoechst dye. Ten minutes after induction of anesthesia, animals were placed on a platform heated to 37°C. A small incision was made in the abdomen and a loop of terminal ileum was exposed and opened longitudinally. The contents were then removed. The platform was then transferred to a FV1000MPE Twin upright multiphoton (Olympus) heated stage, and images collected with time lapse of ±30 s with a total acquisition time of 20 min.

Whole-mount tissue imaging

Imaging of terminal ileum and duodenum was performed as previously described (*20*). Tissues were isolated from TCRγδ-GFP after intravenous injection of Hoechst dye. Contents were removed, and tissue was fixed in 4% PFA overnight at 4°C. Tissues were washed in PBS and placed in FocusClear (Celeplorer Labs Co) solution for 30 min at room temperature. Samples were then mounted on 3D printed slides, and imaging was performed on an Olympus FV1000 upright microscope with a 25X 1.05 NA Plan water-immersion objective and a Mai-Tai DeepSee Ti-Sapphire laser (Spectraphysics).

T cell imaging analysis

T cells located in the lamina propria (dense nucleated area below epithelial basement membrane) where manually counted with Fiji Cell Counter, area scanned from each tissue was 509×509 μm over 41 *z*-stacks of 5-μm step size, starting in the tip of the villus down to the crypts. The total T cell count was performed with Fiji TrackMate v5.1 (*45*) based on a cell

size of 10 μm and GFP signal threshold of 1500 units over all *z*-planes. Total nucleated cells were counted with Fiji TrackMate v5.1 with cell size of 10 μm and DAPI signal threshold of 500 units over all *z*-planes.

RNA FISH

An RNAscope Multiplex Fluorescent V2 (ACD, 323100) detection kit was used according to the manufacturer's instructions. Paraffin-embedded sections were boiled in the target retrieval solution at approximately 100°C for 15 min and incubated in Protease Plus solution at 40°C for 15 min. Probes for the following genes in *Mus musculus* were used: Mm-Sis (573021), Mm-Slc2a2-E11-C2 (439891-C2), and Mm-Slc5a1-C3 (468881-C3), and slides were stained with DAPI. Images and *z*-stacks were acquired with a 40X 1.3 NA oil immersion objective (Zeiss) using a Zeiss LSM900 confocal microscope with Airyscan 2 and Zen software (Zeiss). When indicated, maximum intensity projections were generated using Zen.

Statistics

With the exception of sequencing analysis, all statistical analyses were performed in GraphPad Prism7. Statistical information is included in figure legends.

Plate-based single-cell RNA-seq and analysis

Plate-based single cell RNA-seq was performed as previously described (*15*). RNA-seq libraries were constructed following SMART-seq2 protocol (*46*). RNA clean-up was performed using RNACleanXP beads (Agencourt). Reverse transcription was performed using Maxima H-Reverse Transcriptase (ThermoFisher) followed by whole transcription amplification (WTA) using KAPA HiFi HotStart PCR ReadyMix (KAPA Biosystems). Cleanup of WTA products was performed using AMPure XP beads (Agencourt). DNA quantification was performed using a High Sensitivity DNA Qubit kit and Qubit analyzer (Life Technologies). Fragment sizes were assessed with a high-sensitivity DNA chip (Agilent). Indexing and library preparation was performed using the Nextera XT DNA Library Prep Kit (Illumina). The libraries were sequenced on Illumina NextSeq 500 (38×38 bp paired-end run). A total of 1536 cells were sequenced.

Nextseq 500 base call files were demultiplexed into FASTQ files using bcl2fast2 (Illumina). FASTQ files were used to quantify transcripts for each single cell using kallisto (*47*) Transcript TPMs for each gene were summed to obtain gene level TPMs. A matrix containing the TPMs for each gene for each cell was used as input for the single-cell RNA-seq analysis software package Seurat (*48*). Genes were excluded from the analysis if they had the prefix "GM" or were expressed in fewer than 10 cells. Cells were included in the analysis if they had nonzero TPMs for the Tcell associated genes *Ptprc*, *Cd3d*, and *Cd3e* and expressed at least 1000 genes. After quality control, a total of 361 cells were included in the analysis. Seurat was used to classify cells into clusters and to determine what marker genes defined the clusters. The Seurat FindClusters function was run using a resolution parameter of 0.6. t-SNE and Violin Plots were created using Seurat.

Bulk RNA-seq and analysis

RNA was isolated from sorted T cells using RNEasy Plus Micro Kit (Qiagen), and library preparation performed using SMART-seq2 protocol as described above. RNA was isolated from epithelial cells using DirectZol RNA Miniprep Plus Kit with on-column DNAse digestion according to the manufacturer's instructions (Zymo). Sequencing libraries were constructed using Illumina TruSeq Library Prep Kit and sequenced on Illumina NextSeq 500 (38×38 bp paired-end run).

Sequencing reads were aligned to the mm10 mouse transcriptome (GRCm38 ensembl; cDNA and ncRNA) and quantified by Kallisto (v0.45.0) with a k-mer index 25 and 60 bootstrapping (*47*). The expression of transcript was calculated in TPM (transcripts per million). When multiple transcripts match to the same gene, the expression of the gene is calculated by summing the TPM of all matched transcripts. TPMs of 3 to 4 biological replicates were averaged for each sample. Statistical analyses for differentially expressed genes were performed by Sleuth (*49*).

Droplet-based scRNA-seq and analysis

Single-cell suspensions were loaded onto 3′ library chips as per the manufacturer's protocol for the Chromium Single Cell 3′ Library (V3) (10X Genomics; PN-120233). Briefly, single cells were partitioned into Gel Beads in Emulsion (GEMs) in the Chromium instrument with cell lysis and barcoded reverse transcription of RNA, followed by amplification, enzymatic fragmentation and 5′ adaptor and sample index attachment. Each 10X channel contained either one mouse or a pool of three mice for each condition to account for variations between samples and were loaded on Chromium Single Cell Platform. In addition, both the epithelial fraction and the lamina propria fraction were loaded to the same 10X channel with 7:1 ratio, receptively. An input of 10,000 single cells per sample was added to each channel with a recovery rate of approximately 5000 cells per sample. Libraries were sequenced on an Illumina Nextseq.

Processing FASTQ reads into gene expression matrices

Cell Ranger v2.0 and Cumulus v0.7.0 (*50*) were used to demultiplex the FASTQ reads, align them to the mm10 mouse transcriptome, and to generate the feature-count matrix for the cell-hashing data, using the "cumulus_hashing_cite_seq" workflow described in the Cumulus documentation.

The output of this pipeline is a digital gene expression (DGE) matrix for each sample, which records the number of UMIs for each gene that are associated with each cell barcode. As described previously (*51*), DGE matrices were filtered to remove low quality cells, defined as cells in which fewer than 500 different genes were detected. A total of 122,492 cells were used for downstream analysis. To account for differences in sequencing depth across cells, UMI counts were normalized by the total number of UMIs per cell and converted to transcripts-per-10,000 (henceforth "TP10K").

Cell clustering overview

To cluster single cells into distinct cell subsets, we followed a previously outlined general procedure (*15*) with additional modifications. This workflow includes the following steps: partitioning cells into epithelial, stromal, and immune compartments, followed by clustering the cells within each compartment, which entails the selection of "variable" genes, batch correction, dimensionality reduction (PCA), and graph clustering. Each step of this workflow is detailed below.

Partitioning cells into epithelial, stromal, and immune compartments

Cells were partitioned into epithelial, stromal, and immune compartments based on the expression of known marker genes. First, we clustered the cells by their gene expression profiles (with the clustering procedure below). The clusters were scored for the following gene signatures: epithelial cells (*Epcam*, *Krt8*, and *Krt18*), stromal cells (*Col1Aa1*, *COl1a2*, *COl6a1*, *COl6a2*, *Vwf*, *Plvap*, *Cdh5,* and *S100b*), and immune cells (*Cd52*, *Cd2*, *Cd3d*, *Cd3g*, *Cd3e*, *Cd79a*, *Cd79b*, *Cd14*, *Cd16*, *Cd68*, *Cd83*, *Csf1r*, and *Fcer1g*). Signature scores were calculated as the mean $\log_2$(TP10K+1) across all genes in the signature. Each cluster was assigned to the compartment of its maximal score and all cluster assignments were manually inspected to ensure the accurate segregation of cells. Finally, the cells within each compartment were assembled into three DGE matrices, comprising all epithelial cells, all stromal cells, and all immune cells. The epithelial cells were retained for further downstream analysis.

Variable gene selection

To identify variable genes within a sample, we first calculated the mean (μ) and the coefficient of variation (CV) of expression of each gene. Genes were then grouped into 20 equal-frequency bins (ventiles) according to their mean expression levels. LOESS regression was used to fit the relationship, log(CV) ~ log(μ), and the 1500 genes with the highest residuals were evenly

sampled across these expression bins. To extend this approach to multiple samples, we performed variable gene selection separately for each sample to prevent "batch" differences between samples from unduly impacting the variable gene set. A consensus list of 1500 variable genes was then formed by selecting the genes with the greatest recovery rates across samples, with ties broken by random sampling. This consensus gene set was then pruned through the removal of all ribosomal, mitochondrial, immunoglobulin, and HLA genes, which were found to induce unwanted batch effects in some samples in downstream clustering steps.

Batch correction

We observed substantial variability between cells that had been obtained from different mice, which likely reflects a combination of technical and biological differences. In some cases, these "batch effects" led to cells clustering first by mouse, rather than by cell type or cell state.

To eliminate these batch differences, we ran ComBat (*52*) with default parameters on the $\log_2$(TP10K+1) expression matrix, allowing cells to be clustered by cell type or cell state. Importantly, these batch-corrected data were only used for the PCA and all steps relying on PCA (e.g., clustering, diffusion map, t-SNE visualization); all other analyses (e.g., differential expression analysis) were based on the original expression data.

Dimensionality reduction, graph clustering, and t-SNE visualization

We ran low-rank PCA on the variable genes of the batch-corrected expression matrix, chosen as described above. We then applied Phenograph (*53*) to the k-NN graph defined using PCs 1 to 20 and k = 250, which was selected through close inspection of the data. Finally, the Barnes–Hut t-distributed stochastic neighbor embedding (t-SNE) algorithm was run on the PCs with perplexity = 20 and for 1000 iterations to produce two-dimensional embeddings of the data for visualization.

Identifying statistically significant differences in cell proportions

A major concern with the comparison of cell proportions in scRNA-Seq data are that they are not independent of each other. Because all proportions sum to 1, an increase in the proportion of one cell subset will necessarily lead to a decrease in the proportions of other cell subsets. To account for these dependencies, we used a Dirichlet-multinomial regression model, which tests for differences in cell composition between conditions (e.g., high-carbohydrate diet versus high-protein diet), while accounting for the proportions of all of the other cell subsets.

REFERENCES AND NOTES

1. W. H. Karasov, C. Martínez del Rio, E. Caviedes-Vidal, Ecological physiology of diet and digestive systems. *Annu. Rev. Physiol.* **73**, 69–93 (2011). doi: 10.1146/annurev-physiol-012110-142152; pmid: 21314432
2. W. H. Karasov, A. E. Douglas, Comparative digestive physiology. *Compr. Physiol.* **3**, 741–783 (2013). pmid: 23720328
3. J. B. Furness, The enteric nervous system and neurogastroenterology. *Nat. Rev. Gastroenterol. Hepatol.* **9**, 286–294 (2012). doi: 10.1038/nrgastro.2012.32; pmid: 22392290
4. D. P. Hoytema van Konijnenburg, D. Mucida, Intraepithelial lymphocytes. *Curr. Biol.* **27**, R737–R739 (2017). doi: 10.1016/j.cub.2017.05.073; pmid: 28787597
5. F. M. Gribble, F. Reimann, Function and mechanisms of enteroendocrine cells and gut hormones in metabolism. *Nat. Rev. Endocrinol.* **15**, 226–237 (2019). doi: 10.1038/s41574-019-0168-8; pmid: 30760847
6. L. G. van der Flier, H. Clevers, Stem cells, self-renewal, and differentiation in the intestinal epithelium. *Annu. Rev. Physiol.* **71**, 241–260 (2009). doi: 10.1146/annurev.physiol.010908.163145; pmid: 18808327
7. K. E. Barrett, *Gastrointestinal Physiology* (McGraw Hill Education/Medical, 2014).
8. W. F. Boron, E. L. Boulpaep, Eds., *Medical Physiology* (Saunders/Elsevier, 2012).
9. B. Misselwitz, M. Butter, K. Verbeke, M. R. Fox, Update on lactose malabsorption and intolerance: Pathogenesis, diagnosis and clinical management. *Gut* **68**, 2080–2091 (2019). doi: 10.1136/gutjnl-2019-318404; pmid: 31427404
10. K. Mochizuki, K. Honma, M. Shimada, T. Goda, The regulation of jejunal induction of the maltase-glucoamylase gene by a high-starch/low-fat diet in mice. *Mol. Nutr. Food Res.* **54**, 1445–1451 (2010). doi: 10.1002/mnfr.200900467; pmid: 20425755
11. T. Goda, F. Raul, F. Gossé, O. Koldovský, Effects of a high-protein, low-carbohydrate diet on degradation of sucrase-isomaltase in rat jejunoileum. *Am. J. Physiol.* **254**, G907–G912 (1988). pmid: 3287954
12. J. P. Cézard, J. P. Broyart, P. Cuisinier-Gleizes, H. Mathieu, Sucrase-isomaltase regulation by dietary sucrose in the rat. *Gastroenterology* **84**, 18–25 (1983). doi: 10.1016/S0016-5085(83)80161-9; pmid: 6847846
13. T. Goda, Regulation of the expression of carbohydrate digestion/absorption-related genes. *Br. J. Nutr.* **84** (suppl. 2), S245–S248 (2000). doi: 10.1079/096582197388626; pmid: 11242478
14. M. R. Howitt *et al.*, Tuft cells, taste-chemosensory cells, orchestrate parasite type 2 immunity in the gut. *Science* **351**, 1329–1333 (2016). doi: 10.1126/science.aaf1648; pmid: 26847546
15. A. L. Haber *et al.*, A single-cell survey of the small intestinal epithelium. *Nature* **551**, 333–339 (2017). doi: 10.1038/nature24489; pmid: 29144463
16. J. von Moltke, M. Ji, H. E. Liang, R. M. Locksley, Tuft-cell-derived IL-25 regulates an intestinal ILC2-epithelial response circuit. *Nature* **529**, 221–225 (2016). doi: 10.1038/nature16161; pmid: 26675736
17. C. Schneider *et al.*, A metabolite-triggered tuft cell-ILC2 circuit drives small intestinal remodeling. *Cell* **174**, 271–284.e14 (2018). doi: 10.1016/j.cell.2018.05.014; pmid: 29887373
18. M. Biton *et al.*, T helper cell cytokines modulate intestinal stem cell renewal and differentiation. *Cell* **175**, 1307–1320.e22 (2018). doi: 10.1016/j.cell.2018.10.008; pmid: 30392957
19. A. E. Moor *et al.*, Spatial reconstruction of single enterocytes uncovers broad zonation along the intestinal villus axis. *Cell* **175**, 1156–1167.e15 (2018). doi: 10.1016/j.cell.2018.08.063; pmid: 30270040
20. D. P. Hoytema van Konijnenburg *et al.*, Intestinal epithelial and intraepithelial T cell crosstalk mediates a dynamic response to infection. *Cell* **171**, 783–794.e13 (2017). doi: 10.1016/j.cell.2017.08.046; pmid: 28942917
21. P. Vantourout, A. Hayday, Six-of-the-best: Unique contributions of γδ T cells to immunology. *Nat. Rev. Immunol.* **13**, 88–100 (2013). doi: 10.1038/nri3384; pmid: 23348415
22. H. Gehart, H. Clevers, Tales from the crypt: New insights into intestinal stem cells. *Nat. Rev. Gastroenterol. Hepatol.* **16**, 19–34 (2019). doi: 10.1038/s41575-018-0081-y; pmid: 30429586
23. L. A. Zenewicz *et al.*, Innate and adaptive interleukin-22 protects mice from inflammatory bowel disease. *Immunity* **29**, 947–957 (2008). doi: 10.1016/j.immuni.2008.11.003; pmid: 19100701
24. X. Wang *et al.*, Interleukin-22 alleviates metabolic disorders and restores mucosal immunity in diabetes. *Nature* **514**, 237–241 (2014). doi: 10.1038/nature13564; pmid: 25119041
25. C. A. Lindemans *et al.*, Interleukin-22 promotes intestinal-stem-cell-mediated epithelial regeneration. *Nature* **528**, 560–564 (2015). doi: 10.1038/nature16460; pmid: 26649819
26. K. Gronke *et al.*, Interleukin-22 protects intestinal stem cells against genotoxic stress. *Nature* **566**, 249–253 (2019). doi: 10.1038/s41586-019-0899-7; pmid: 30700914
27. S. Sawa *et al.*, RORγt+ innate lymphoid cells regulate intestinal homeostasis by integrating negative signals from the symbiotic microbiota. *Nat. Immunol.* **12**, 320–326 (2011). doi: 10.1038/ni.2002; pmid: 21336274
28. C. E. O'Leary, C. Schneider, R. M. Locksley, Tuft cells-systemically dispersed sensory epithelia integrating immune and neural circuitry. *Annu. Rev. Immunol.* **37**, 47–72 (2019). doi: 10.1146/annurev-immunol-042718-041505; pmid: 30379593
29. M. G. Constantinides *et al.*, MAIT cells are imprinted by the microbiota in early life and promote tissue repair. *Science* **366**, eaax6624 (2019). doi: 10.1126/science.aax6624; pmid: 31649166
30. M. Ribeiro *et al.*, Meningeal γδ T cell-derived IL-17 controls synaptic plasticity and short-term memory. *Sci. Immunol.* **4**, eaay5199 (2019). doi: 10.1126/sciimmunol.aay5199; pmid: 31604844
31. M. J. Hong *et al.*, Protective role of γδ T cells in cigarette smoke and influenza infection. *Mucosal Immunol.* **11**, 894–908 (2018). doi: 10.1038/mi.2017.93; pmid: 29091081
32. G. Crawford *et al.*, Epithelial damage and tissue γδ T cells promote a unique tumor-protective IgE response. *Nat. Immunol.* **19**, 859–870 (2018). doi: 10.1038/s41590-018-0161-8; pmid: 30013146
33. A. C. Kohlgruber *et al.*, γδ T cells producing interleukin-17A regulate adipose regulatory T cell homeostasis and thermogenesis. *Nat. Immunol.* **19**, 464–474 (2018). doi: 10.1038/s41590-018-0094-2; pmid: 29670241
34. S. He *et al.*, Gut intraepithelial T cells calibrate metabolism and accelerate cardiovascular disease. *Nature* **566**, 115–119 (2019). doi: 10.1038/s41586-018-0849-9; pmid: 30700910
35. J. G. Markle *et al.*, γδ T cells are essential effectors of type 1 diabetes in the nonobese diabetic mouse model. *J. Immunol.* **190**, 5392–5401 (2013). doi: 10.4049/jimmunol.1203502; pmid: 23626013
36. P. Mehta, A. M. Nuotio-Antar, C. W. Smith, γδ T cells promote inflammation and insulin resistance during high fat diet-induced obesity in mice. *J. Leukoc. Biol.* **97**, 121–134 (2015). doi: 10.1189/jlb.3A0414-211RR; pmid: 25395302
37. B. E. Willcox, C. R. Willcox, γδ TCR ligands: The quest to solve a 500-million-year-old mystery. *Nat. Immunol.* **20**, 121–128 (2019). doi: 10.1038/s41590-018-0304-y; pmid: 30664765
38. A. Bas *et al.*, Butyrophilin-like 1 encodes an enterocyte protein that selectively regulates functional interactions with T lymphocytes. *Proc. Natl. Acad. Sci. U.S.A.* **108**, 4376–4381 (2011). doi: 10.1073/pnas.1010647108; pmid: 21368163
39. D. Melandri *et al.*, The γδTCR combines innate immunity with adaptive immunity by utilizing spatially distinct regions for agonist selection and antigen responsiveness. *Nat. Immunol.* **19**, 1352–1365 (2018). doi: 10.1038/s41590-018-0253-5; pmid: 30420626
40. K. Mao *et al.*, Innate and adaptive lymphocytes sequentially shape the gut microbiota and lipid metabolism. *Nature* **554**, 255–259 (2018). doi: 10.1038/nature25437; pmid: 29364878
41. J. Talbot *et al.*, VIP-producing enteric neurons interact with innate lymphoid cells to regulate feeding-dependent intestinal epithelial barrier functions. bioRxiv 721464 [Preprint] 7 December 2019. .doi: 10.1101/721464
42. J. Talbot *et al.*, Feeding-dependent VIP neuron-ILC3 circuit regulates the intestinal barrier. *Nature* **579**, 575–580 (2020). doi: 10.1038/s41586-020-2039-9; pmid: 32050257
43. P. S. Korpe, W. A. Petri Jr., Environmental enteropathy: Critical implications of a poorly understood condition. *Trends Mol. Med.* **18**, 328–336 (2012). doi: 10.1016/j.molmed.2012.04.007; pmid: 22633998
44. S. P. Spencer *et al.*, Adaptation of innate lymphoid cells to a micronutrient deficiency promotes type 2 barrier immunity. *Science* **343**, 432–437 (2014). doi: 10.1126/science.1247606; pmid: 24458645
45. J. Y. Tinevez *et al.*, TrackMate: An open and extensible platform for single-particle tracking. *Methods* **115**, 80–90 (2017). doi: 10.1016/j.ymeth.2016.09.016; pmid: 27713081

46. S. Picelli *et al*., Full-length RNA-seq from single cells using Smart-seq2. *Nat. Protoc.* **9**, 171–181 (2014). doi: 10.1038/nprot.2014.006; pmid: 24385147
47. N. L. Bray, H. Pimentel, P. Melsted, L. Pachter, Near-optimal probabilistic RNA-seq quantification. *Nat. Biotechnol.* **34**, 525–527 (2016). doi: 10.1038/nbt.3519; pmid: 27043002
48. A. Butler, P. Hoffman, P. Smibert, E. Papalexi, R. Satija, Integrating single-cell transcriptomic data across different conditions, technologies, and species. *Nat. Biotechnol.* **36**, 411–420 (2018). doi: 10.1038/nbt.4096; pmid: 29608179
49. H. Pimentel, N. L. Bray, S. Puente, P. Melsted, L. Pachter, Differential analysis of RNA-seq incorporating quantification uncertainty. *Nat. Methods* **14**, 687–690 (2017). doi: 10.1038/nmeth.4324; pmid: 28581496
50. J. T. Gaublomme *et al*., Nuclei multiplexing with barcoded antibodies for single-nucleus genomics. *Nat. Commun.* **10**, 2907 (2019). doi: 10.1038/s41467-019-10756-2; pmid: 31266958
51. C. S. Smillie *et al*., Intra- and inter-cellular rewiring of the human colon during ulcerative colitis. *Cell* **178**, 714–730.e22 (2019). doi: 10.1016/j.cell.2019.06.029; pmid: 31348891
52. W. E. Johnson, C. Li, A. Rabinovic, Adjusting batch effects in microarray expression data using empirical Bayes methods. *Biostatistics* **8**, 118–127 (2007). doi: 10.1093/biostatistics/kxj037; pmid: 16632515
53. J. H. Levine *et al*., Data-driven phenotypic dissection of AML reveals progenitor-like cells that correlate with prognosis. *Cell* **162**, 184–197 (2015). doi: 10.1016/j.cell.2015.05.047; pmid: 26095251
54. W. Huang, B. T. Sherman, R. A. Lempicki, Systematic and integrative analysis of large gene lists using DAVID bioinformatics resources. *Nat. Protoc.* **4**, 44–57 (2009). doi: 10.1038/nprot.2008.211; pmid: 19131956

ACKNOWLEDGMENTS

We thank all members of the Medzhitov laboratory for discussions and C. Annicelli, S. Cronin, and C. Zhang for assistance with animal care and husbandry. We thank F. Carvalho for assistance with image analysis, W. Garrett (Harvard University) for *Trpm5*$^{-/-}$ mice, and C. Wilen (Yale University) for *Pou2f3*$^{-/-}$ mice. **Funding:** The R.M. laboratory is supported by the Howard Hughes Medical Institute, Blavatnik Family Foundation, Food Allergy Science Initiative, and a grant form NIH (AI144152-01). Z.A.S. was supported by the National Science Foundation Graduate Research Fellowship Program under grant DGE1122492. Any opinions, findings, and conclusions or recommendations expressed in this material are those of the author(s) and do not necessarily reflect the views of the National Science Foundation. D.M. was supported by the National Institute of Diabetes and Digestive and Kidney Diseases award R01DK113375. W.K-H. was supported by NIH under award F32-AI143141. J.L. was supported by postdoctoral fellowships from the International Human Frontier Science Program Organization (LT000037/2018-L) and Jane Coffin Childs Memorial Fund. R.K.Z. was supported by NIH F32-DK125089. R.M. and A.R. are investigators of the Howard Hughes Medical Institute. **Author contributions:** Z.A.S. and R.M. conceived the study. Z.A.S., W.K-H., M.B., B.S.R., and R.K.Z. performed experiments with help from S.D.P., K.I-W., N.H.P., and S.R.; Z.A.S., W.K-H., J.L., C.S., B.S.R., S.D.P., and R.P. analyzed data. Z.A.S. and R.M. wrote the manuscript, with input from N.P., A.W., D.M., and A.R. **Competing interests:** A.R. is a cofounder and equity holder of Celsius Therapeutics, is an equity holder in Immunitas, and was an SAB member of ThermoFisher Scientific, Syros Pharmaceuticals, Neogene Therapeutics, and Asimov until 31 July 2020. From 1 August 2020, A.R. is an employee of Genentech. Authors declare no other competing interests. **Data and materials availability:** Sequencing data are available from the National Center for Biotechnology Information Gene Expression Omnibus (GSE145857). All data are available in the main text or the supplementary materials.

SUPPLEMENTARY MATERIALS

science.sciencemag.org/content/371/6535/eaba8310/suppl/DC1
Figs. S1 to S14
Tables S1 to S6
Movie S1
MDAR Reproducibility Checklist

View/request a protocol for this paper from *Bio-protocol*.

8 January 2020; resubmitted 2 November 2020
Accepted 19 January 2021
10.1126/science.aba8310

Science

γδ T cells regulate the intestinal response to nutrient sensing

Zuri A. Sullivan, William Khoury-Hanold, Jaechul Lim, Chris Smillie, Moshe Biton, Bernardo S. Reis, Rachel K. Zwick, Scott D. Pope, Kavita Israni-Winger, Roham Parsa, Naomi H. Philip, Saleh Rashed, Noah Palm, Andrew Wang, Daniel Mucida, Aviv Regev and Ruslan Medzhitov

Science **371** (6535), eaba8310.
DOI: 10.1126/science.aba8310

γδ T cells link immunity to nutrition

Gamma delta (γδ) T cells are immune cells best known for host barrier defenses in epithelial tissues. Sullivan *et al.* discovered a previously unrecognized role for γδ T cells in sensing nutrient uptake in the small intestine (see the Perspective by Talbot and Littman). The researchers analyzed mice fed a high-carbohydrate versus a high-protein diet and observed remodeling of the small intestinal epithelium in response to dietary carbohydrates. Nutrient availability triggered an epithelial–immune cell circuit that was required for digestion and absorption of carbohydrates. Intestinal γδ T cells regulated the expression of a carbohydrate transcriptional program by limiting interleukin-22 production from type 3 innate lymphoid cells. These findings may also provide insights into how γδ T cells modulate metabolic disease.

Science, this issue p. eaba8310; see also p. 1202